International Journal Of Core Engineering & Management
Volume-6, Issue-7, 2020 ISSN No: 2348-9510

WIND TUNNEL VORTEX FLOW VISUALIZATION AND TRACKING ON A DELTA WING AT HIGH ANGLES OF ATTACK

Salaheldin H. Omar
Professor of Aerospace and Autonomous Systems Engineering and former Chair;
Talent and Technology Creativity Unit,
University of Tabuk, Saudi Arabia.
salaheldin.omar@outlook.com

Saad Adam
Assistant Professor, Faculty of Engineering, University of Tobruk,
Libya, saadadam22@gmail.com

Ashraf M. Zobi
M.Sc.-Eng., Head of Petroleum Engineering Dept.,
University of Tobruk, Libya,
a.zuby@eng.tu.edu.ly

Fatima Omar
Faculty of Computer and Information Science,
fatma20191704021@cis.asu.edu.eg

Fadi Alshamari
Eng., Prince Sultan Defense Studies & Research Center, Riyadh, Saudi Arabia,
fadi.alshammari@psdsarc.org

Abstract

The fluid flow phenomena associated with delta wings have dominant effects on the performance of high agility aircrafts at super maneuvering rates and slender body of revolution. They help also to understand the physics of dynamical meteorology, physical oceanography and enhancing the fuel/air mixing process inside the internal combustion chambers. This investigation is dealing with wind tunnel flow visualization over a slender delta wing using smoke/laser-light-sheet flow visualization technique and liquid crystals for surface streamlines flow visualizations and surface shear stresses at U_∞ = 48 m/s for different angles of attack from zero up to 45 degrees. The lateral and vertical development of the vortex subcore position over the leeward side of the wing has been predicted. The position of the laminar turbulent transition of the secondary separation line over the wing with increasing the angle of attack has been predicted. The lateral position of the secondary and tertiary separations has been predicted for different angles of attack. The simultaneous existing of both bubble and spiral type vortex breakdowns have been observed and their locations have been predicted. The development of the trailing edge vortices and their trajectory from the pressure side of the wing to the leeward side at the trailing edge moving downstream and upstream around the primary vortex have been observed.

International Journal Of Core Engineering & Management
Volume-6, Issue-7, 2020 ISSN No: 2348-9510

Keywords: Vortex Flow, Vortex Breakdown, Vortex Dynamics, Delta Wing, Super Maneuvering Aircraft, High Agility Aircraft, Slender Body of Revolution, Wind Tunnel, Flow Visualization, Liquid Crystals, Smoke, Laser Light Sheet, Surface Stream Lines, Surface Shear Stress

Nomenclatures

Cr - Wing root chord
Re - Reynolds number based on chord length of the wing
Λ - Aspect ratio
r - Radius of viscous sub core
λ - wave length
ρ - Fluid density
ρ_o - Reference density (a pure constant)
k - Number of waves
δ - Local vortices thickness (vertical extent of mixing zone)
$\Delta \rho$ - Density difference of two adjacent fluid streams
ΔU - Difference between flow Velocities of two adjacent fluid streams
ω - Angular velocity
R - Radial distance from the centre of the vortex core
$g' = g\ (\rho 2 - \rho 1)$ *is the reduced gravity*
S - Local wing span
$U\infty$ - Free stream speed
x - Local chord-wise distance from wing apex
y - Local span-wise distance from wing root "from wing line of symmetry"
Z - Local distance above wing surface
h - Maximum wing profile thickness
α - Wing angle of attack
α_C - Vortex-core angle of attack
Λ_C - Vortex-core sweep angle
β - Wing angle side slip
ΛLE - Wing sweep back angle
Vswirl - Vortex swirl velocity
Vaxial - Vortex axial velocity
ϕ - Swirl angle = tan-1 (Vswirl / Vaxial)
Cp - Surface pressure coefficient

I. INTRODUCTION

1.1. The Vortex flow

Vortex flow is an important phenomenon associated with high agility aircrafts at super maneuvering rates, slender body of revolutions, highly swept back wings and delta wing, dynamical meteorology covering Thunderstorms, Sea breeze, Tornado, Hurricane, Mountain waves, and physical oceanography including oceanic waves, vortices, currents, long oceanic waves, atmospheric convection, and natural oscillations in air-sea interactions. High agility

International Journal Of Core Engineering & Management
Volume-6, Issue-7, 2020 ISSN No: 2348-9510

aircrafts maneuvering at high angles of attack might be affected by Asymmetrical and antisymmetrical vortex flow and breakdown leading to large side forces and yawing moments beyond the maximum moments affordable by the control surfaces. Flow visualization occurs naturally by airborne dust particles in nature and artificially using different methods and techniques inside and outside wind tunnels.

1.2. Vortices over delta wings;

In a homogeneous fluid, mixing requires enough energy necessary to overcome mechanical frictions, but in a stratified fluid additional energy is necessary to raise heavy fluid parcels and lower light fluid parcels against buoyancy forces increasing the potential energy and therefore the mixing can proceed spontaneously if the reduction in the kinetic-energy exceeds the increase in the potential-energy. Mixing of fluid parcels can be performed only if the initial density-difference is small enough to avoid an insurmountable gravitational barrier [1, 2] Thorpe, S. A. (1968, 1971), or if the initial velocity-shear is large enough to provide the necessary energy for the fluid mixing process to take place. The ratio between potential and kinetic energies has been defined as Richardson number "Ri", with the numerator is the potential-energy barrier that mixing process must overcome to be performed and the denominator is the available kinetic energy of the shear flow.

Richradson number = $(g/\rho_o)\,\Delta\rho\,\delta/\Delta U^2$ after [3] Richardson Lewis Fry (1922)

Kelvin-Helmholtz instability was first studied by Taylor in 1915 [4] Taylor, G. I., (1931) summarizing that Richardson number must be less than ¼ for instability to take place, otherwise, the mixing process occurs only locally in a vicinity of the initial interface and will not therefore be able to spread over the whole system. The flow streamlines of both sides of delta wing join at the separation line along the wing leading edge forming separated free shear layer of two separated adjacent streams of different velocities, namely the lower velocity stream from the pressure side, and the higher velocity stream from the suction leeside. The different velocities of the two parallel streams of the separated shear layer initiate inviscid instability of a constant-vorticity layer in the interfacial region inside the free shear layer and generate laminar small waves which distorts the boundaries of the region containing the vorticities as in figure 1(a).

The perturbations induce vertical velocities which force the perturbations and waves to grow into discrete vortices and therefore increasing the thickness of the free shear layer by moving away from the leading edge, figure 1 (b). These spatially growing mixing layers are characterized by the formation of big spiral vortices resulting from Kelvin-Helmholtz instability. Each vorticity tends to entrain the other neighbored vorticity under the influence of their induced velocity forcing both vortices to rotate around one another in pair due to the nonlinear interaction. Every vorticity rotate slower at its outer part than close to the center initiating tails as shown in figure 1-C which merge into spirals during the pairing [5] Piercy N. A. V. (1923), [6] Winant, C. et al (1974). The interfacial region of constant vorticity becomes periodically fatter and thinner, figure 1 (c) and the pairing process starts. The pairing process amplifies the spatial and irregularities in the vortex structure and increasing the variations in the length and strength of the vortex cores which are continually rotating around one another in pairs forming the rotating vortex lumps in the interfacial region of the free shear layer figure 1(d) and figure 2. The free shear layer rolls up into a vortex core by the impact of the vorticity induced flow velocities on both sides of vortex lumps within the free shear layer as shown in figure 1- (d and e), figure 2, and figure 3 of wind tunnel smoke and laser light sheet flow visualization over sharp edged delta wing. The primary vortex can be divided, after [7]

International Journal Of Core Engineering & Management
Volume-6, Issue-7, 2020 ISSN No: 2348-9510

Earnshaw P. (1962), into three regions, namely; the free shear layer, the rotational core, and viscous subcore as shown in figure 2.

The free shear layer rolls up into a vortex core by the impact of the vorticity induced flow velocities on both sides of vortex lumps within the free shear layer as shown in figure 1- (d and e), 2, and figure 3 of wind tunnel smoke and laser light sheet flow visualization over sharp edged delta wing after. The primary vortex can be divided, after [7] Earnshaw P. (1962), into three regions, namely; the free shear layer, the rotational core, and viscous subcore as shown in figure 2. The free shear layer generated at the leading edge rolled up forming the primary vortex induces the outer flow of the primary vortex to reattach on the leeward side of the delta wing and is continually providing the boundary layer after the reattachment line with fresh air of high energy as illustrated in figure 2. The reattached flow moves from the reattachment line outboard toward the leading edge until it separates at the secondary separation line somewhere between the axis of the primary vortex and the leading edge in dependence of the flow condition "laminar/turbulent" forming the secondary vortex. Tertiary vortex may be initiated underneath the secondary vortex with a rotation in the same sense of the primary vortex.

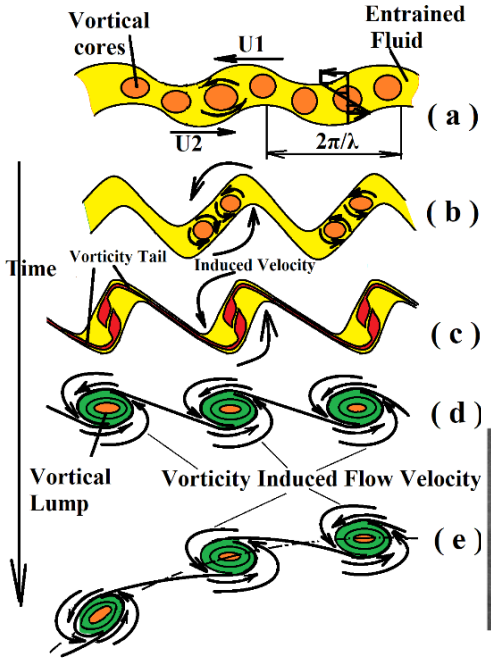

Figure 1 (a-e): Vortex pairing and lumps

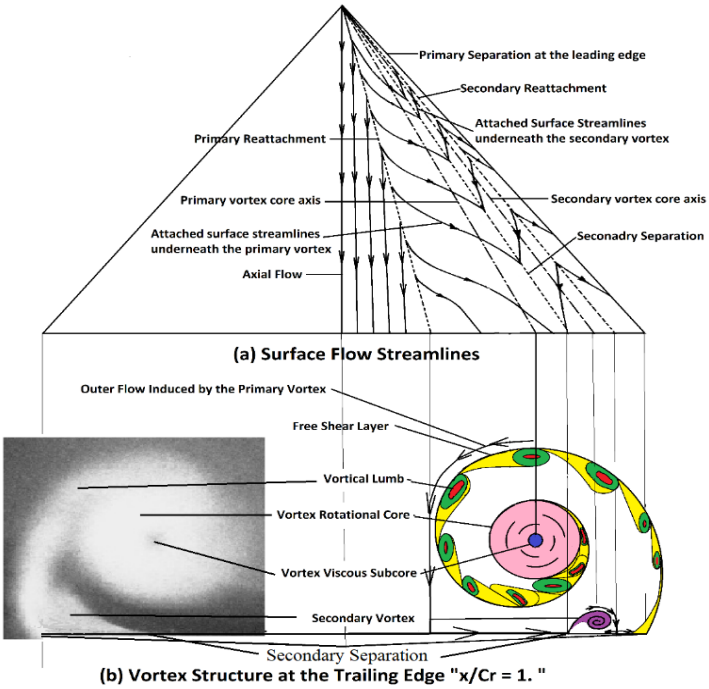

Figure 2: surface flow stream lines and vortex flow of a delta wing

International Journal Of Core Engineering & Management
Volume-6, Issue-7, 2020 ISSN No: 2348-9510

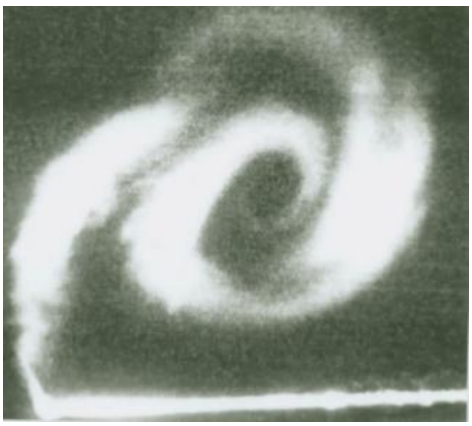

Figure 3: Rolling up of the separated vortex sheet forming the primary vortex over a delta wing

1.3. Laminar / turbulent transition

At higher angle of attack and Reynolds number, a laminar/turbulent transition of the boundary layer in the rear part of the wing provides the reattached flow with higher energy maintaining the flow attached longer distance toward the leading edge at and aft this location forming outboard kink of the secondary separation line at this location and decreasing its distance from the leading edge as in figures 3 and 4 and consequently, the possibility of initiation of tertiary and multiple vortices becomes very hard. A secondary vortex, smaller in size and lower in strength than in the case of laminar boundary layer, is formed leading to greater upward and inward displacements of the primary vortex than for laminar boundary layer [8] Payne F. et al, (1986), [9] Payne F., (1987). The relation between lift and angle of attack is linear for wings of high aspect ratios and nonlinear for wings of low aspect ratios. The nonlinearity, which is initiated by the vortex sheet above the wing, increases with decreasing the aspect ratio. The circulation increases with angle of attack increasing the lift-curve slope and decreases by increasing the sweep angle reducing the lift-curve slope. The secondary vortex undergoes changes, resembling the breakdown phenomena of the primary vortex before it occurs in the primary vortex. The secondary vortex retains its vortex flow structure aft of primary vortex breakdown location [10] Nelson R. and Visser K. (1991). Increasing the Reynolds number results in increasing the unsteady perturbations in the shear layer [11] Riley A. and Lawson V. (1998). [12] Delery J. (1994) suggested that the secondary vortex is not affected by the breakdown of the primary vortex. [13] Huang, X., and Hanff, E. (1998) relates the outboard kink of the secondary separation line to the vortex breakdown, Reverse flow patterns were observed when breakdown was in the apex region. [14] Earnshaw P. and Lawford J. (1964) visualized a "whorl" close to each leading edge in the rear part of the wing.

International Journal Of Core Engineering & Management
Volume-6, Issue-7, 2020 ISSN No: 2348-9510

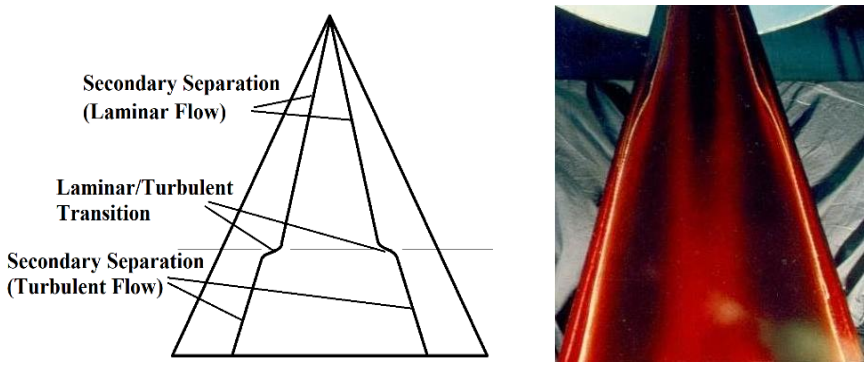

(a) (b)

Figure 3: Laminar/turbulent transition

1.4 Vortex Breakdown

Vortex breakdown is defined by [15] Sarpkaya T. (1971) as an abrupt change in the structure of the vortex core, followed by a growing asymmetric flow around the vortex axis. [16] Leibovich S. (1979) and [17] Garg A. & Leibovich S. (1979) defined vortex breakdown as a disturbance that is characterized by the formation of an internal stagnation point on the vortex axis followed by a reversed flow. Vortex breakdown has many different and contradictory aspects of view and interpretations. Vortex breakdown occurs, after [18] Hall, M. (1972), in dependence of the magnitude of the flow swirling, as an indication of the vorticity shedded in the rolled up free shear layer, and of the external pressure gradient and the degree of the divergence as indication of the vorticity convection along the vortex axis [19] Schade H., Michalke, A. (1962). At a certain angle of attack the increased rate of generation of the vortices shedded in the vortex sheet exceeds the convection of these vortices leading to an increase in the concentrated vortices, which have limits on the their maximum amount of vortices per unit area "critical vortices concentration". By exceeding these limits, the shedded vortices in the rolled up free shear layer cannot be compensated by the convection of the vortices, which is dependent on the increased component of the axial flow velocity by increasing the angle of attack, and gradually, the axial momentum becomes too weak to overcome the adverse pressure gradient, leading to a drastic increase in the interactions among the vortex-outer-core spirals, and to the formation of a stagnation point along the viscous subcore, subsequently, the vortex cannot maintain its organized structure leading to a spiral form or bubble form vortex breakdown, as in figure 4, spreading the vortices over a wider region and the excessive vortices are redistributed in the region aft the vortex breakdown location reducing the vorticity concentration inside the vortex sheet [8, 9] Payne F. M. et al (1986), Payne F. M. (1987) and [20, 21] Faler J. H. et al (1977, 1978).

1.4.1 Types of Vortex Breakdown

Many different types of vortex breakdown have been identified in vortex tube experiments. Lambourne N. C., and Bryer D. W. (1961) [22] were among the first who investigated and defined the types of vortex breakdown on a delta wing as bubble and spiral vortex breakdown. For slender wings at angle of attack only two types of breakdown are generally identified, the bubble and the spiral breakdown, although in reality they may just represent the extremes of the breakdown forms. Vortex breakdown location is not a function of the Reynolds number for sharp edged wings.

International Journal Of Core Engineering & Management
Volume-6, Issue-7, 2020 ISSN No: 2348-9510

1.4.1.1. Spiral breakdown

Lambourne N. C., and Bryer D. W. (1961) [22] characterized the spiral vortex breakdown by a rapid deceleration of the core flow followed by an abrupt kink at which point, the core flow takes the form of a spirals making one or two turns before breaking up into large scale turbulence as shown in figure 6. The breakdown is due to the fact that high velocity vortex core cannot maintain its straight course. The vortex core is, therefore, forced to move outward in an effort to maneuver its way downstream. This outward motion takes the form of a spirals in a direction opposite to the original motion of the upstream vortex, however the winding rotates in the same direction as that of the upstream vortex because the motion of the rotational outer core is consistent with the original sign of vorticity and because of the need to conserve the angular momentum of the fluid particles within the core. Another explanation by Ludwieg H. (1962, 1965) [23, 24] stated that spiral form of breakdown can be explained as a hydrodynamic instability of the approach flow against small helical disturbances, which means that there is at least two different mechanisms for vortex breakdown. Vortex breakdown cannot be explained by one theory only. Spiral vortex breakdown is a result of an instability of the viscous subcore and not the outer vortex layers. Spiral breakdown occurs primarily if the breakdown position is approaching the trailing edge Lambourne N. & Bryer D. (1961) [22], Payne, F. M. (1987) [9] and Faler & Leibovich (1977) [20].

1.4.1.2. Bubble breakdown

Bubble breakdown is characterized by a stagnation point on the vortex axis followed by an oval shaped recirculation zone Payne, F. M. et al (1986) [8]. The upstream half of the recirculation zone is nearly axisymmetric with the flow passing around it, however the downstream half is usually open and irregular with the flow shedding from the aft end as if it were shedding from a blunt solid body in the form of shedded rings. The bubble length is usually two to three times that of the upstream-core diameter as in figure 6. Downstream to the bubble the vortex is turbulent and diffuses rapidly with distance. Bubble breakdown occurs only if the breakdown location is in moving close to the apex Payne, F. M. et al (1986) [8], Payne F. (1987) [9] and Faler J. H., Leibovich S. (1977, 1978) [20, 21].

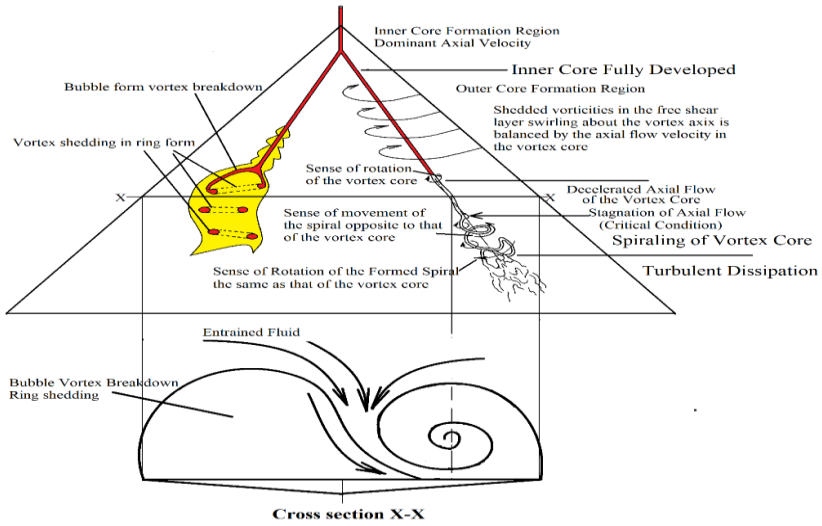

Figure 4: Vortex formation and breakdown over delta wings

International Journal Of Core Engineering & Management
Volume-6, Issue-7, 2020 ISSN No: 2348-9510

II. EXPERIMENTAL SETUP

2.1. Wind tunnel facility and test condition

All experiments were carried out in low speed closed loop water cooled wind tunnel of TU Munich, Germany. The test section of the wind tunnel is open flow test section of 1.2 meter diameter, U∞ = 72 m/s maximum speed, and 0.2-0.3 % turbulence shown in figure 5. The Smoke generator and the laser light sheet instruments are shown in figure 6-a, b

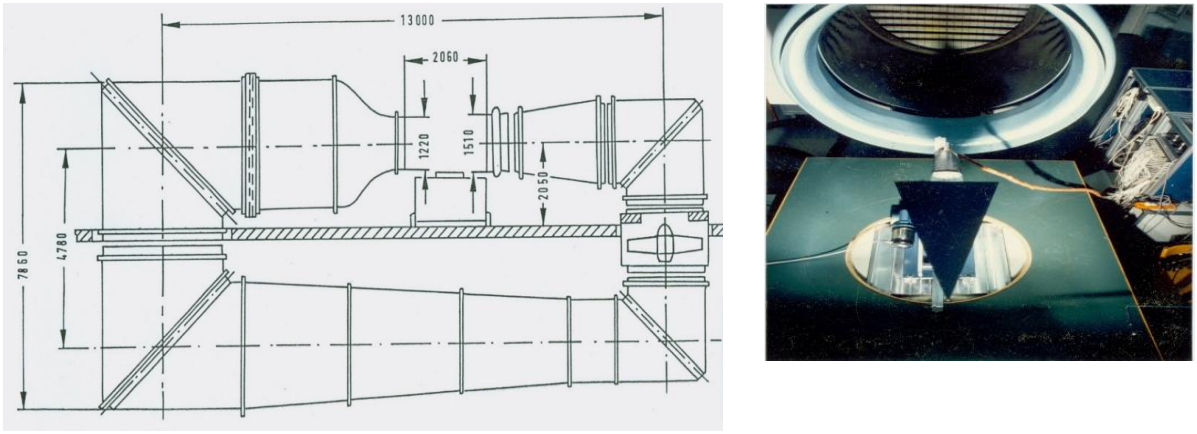

(a) (b)

Figure 5 Wind Tunnel Facility

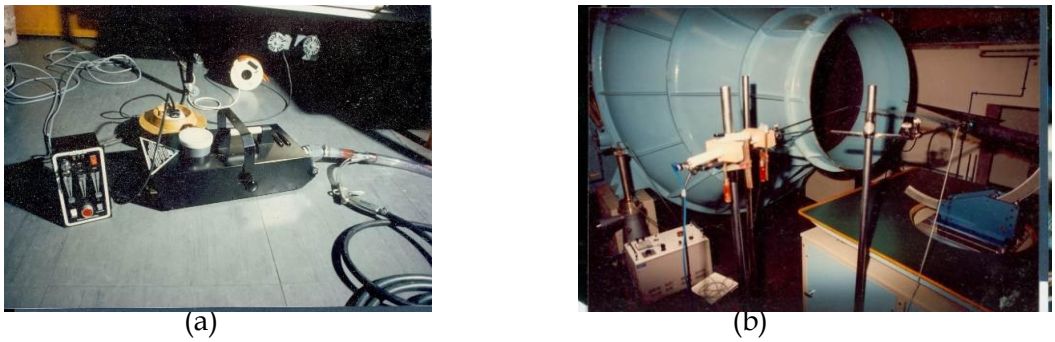

(a) (b)

Figure 6 (a) smoke generator (b) laser light sheet instrumentation

2.2. Wind Tunnel Test Model

The wind tunnel test model is a sharp edged delta wing manufactured from carbon fibers to predict solely the aerodynamic forces by minimizing elastic forces and inertia forces, which interact mutually with the aerodynamic forces changing their predicted values. The development and breakdown of the vortex over the leeside of the delta wing as well as the vortex shedding at very high angles of attack up to 65 degree have been predicted.

The test model is a light weight, stiff, sharp edged delta wing made from carbon fibers of aspect ratio Λ =1, sweep back angle ΛLE of 76 degree, length of 670mm, chord of 335mm and maximum

International Journal Of Core Engineering & Management
Volume-6, Issue-7, 2020 ISSN No: 2348-9510

thickness h of 57mm as shown in figure 7.

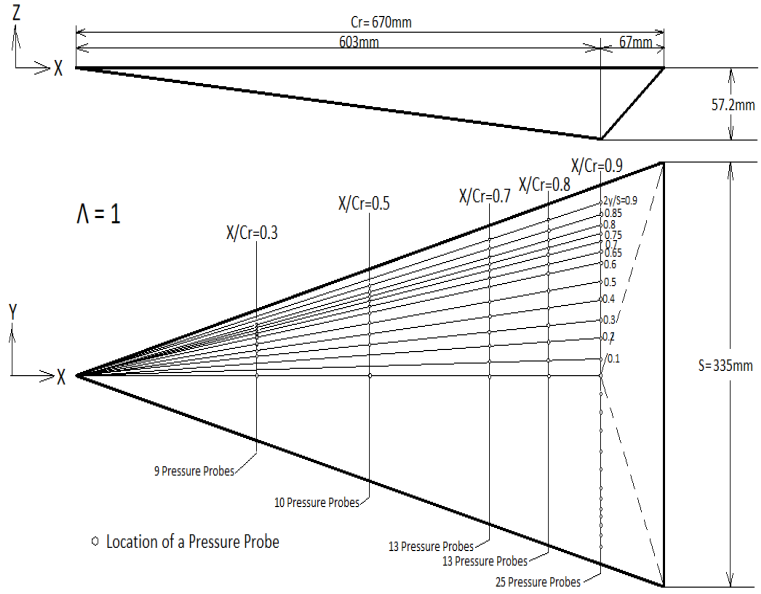

Figure 7 Delta wing dimension and layout of the sensors

Liquid Crystals with rod-shaped molecules are the most commonly used in surface flow visualization, they are arranged in layers with molecules parallel to each other (figure 8-a) and the individual molecules move relatively easily in the direction along their axis independent from the layer structure (figure 8-b) giving different reflections in dependence of the shear stresses.

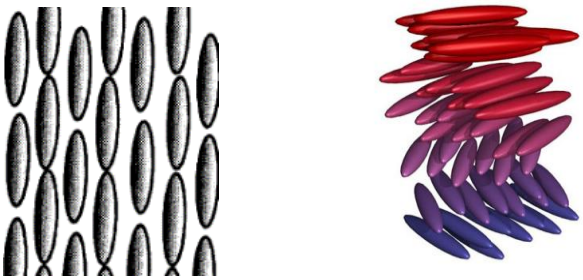

(a) (b)

Figure 8 Liquid Crystal Material (a, b)

The characteristic pitch length of the helical molecular structure of the liquid crystals falls within the wavelength range of the visible spectrum and responds to changes in surface shear stresses [22] Smith, S. C. (1992). The used liquid-crystal mixture in this investigation is the red colored CN/R3 from Hall Crest Company; it is sensitive to shear stresses and insensitive to temperature. A mixture of one part liquid crystals to 5-10 parts solvent, here acetone, was sprayed on the leeward surface of the wing after covering it with special black adhesive paper which is necessary for enhancing color contrast. The solvent evaporates forming uniform thin coat which selectively scatters incident unpolarized white light as discrete colors. For static conditions, where no

dynamic stresses are acting on the liquid crystals, the optimum thickness lies in the range of 0.5 to 1.6 ml/m2. The used coating thickness in this investigation was about 1.3 ml/m2 because thick coating shows, superposed on the enhanced color pattern, a marked stream flow line pattern, similar to that obtained by the oil flow method. The sprayed liquid crystals over the surface tends to flow off the surface during the run of the wind tunnel for long period leading to gradual thinning of the liquid-crystal coat and its complete removal in the high stress regions at the leading edge, underneath vortices, and close to the apex in case of delta wing. Therefore photos have been taken immediately after the surface streamlines are formed in the liquid crystal coating film. The optimum positions of the light source and the camera have been searched and readjusted precisely and repeatedly in positions of minimum specular liquid crystal reflections searching for the optimum angles of illumination and of viewing the maximum light scattering intensity of the liquid crystals.

III. RESULTS AND DISCUSSIONS

At zero angle of attack and free stream speed of $U\infty$ = 48 m/s, the laser light sheet flow visualization pictures in Figure 9-a show a full rolled up vortex at the trailing edge corner (X/Cr=1) at zero angle of attack. The formation of the vortex at zero angle of attack is due to the chambered wing. The development process of the sprayed liquid-crystal film on the leeward side of the wing during speeding up the wind tunnel is illustrated in the figure (1 a-d). Immediately after operating the wind tunnel the response of the liquid crystals is significant in fig 9-b, 10-b, and 15(a-d) through distinct color distributions indicating regions of different shear stresses. Dark areas represents regions of high shear stresses as those underneath the vortices. The stream lines start to form after a while gradually as shown in figure 15 a-d. The liquid crystal sprayed thin sheet on the leeward surface of the wing show a dominant downstream streamlines over the whole wing except close to both leading edges where rolled up vortex flow is present and indicated by dark band extended from the area close to the apex to the trailing edge (figure 10-b). The vortex is stronger and well-formed more close to the trailing edge.

Increasing the angle of attack to 5 degrees at $U\infty$ = 48 m/s result in upstream extension of the region having a full rolled up vortex up to a region close to the apex, at which the vortex core start its formation. The vortex is moved inboard toward the line of symmetry and upward away from the leeward side of the wing from the region close to the apex to the trailing edge as in figure 10 (a). Dark areas represents regions of high shear stresses as those underneath the vortices (figure 10-b).

Additional increase of the angle of attack to 10 degrees at $U\infty$ = 48 m/s results in an additional movement of the vortex inboard to the line of symmetry of the wing and upward from the leeward surface of the wing (figure 11 a). The liquids crystal pictures indicate a straight secondary separation line from a region close to the apex to the trailing edge as in figure 11-b. Dark areas represents regions of high shear stresses as those underneath the vortices.

International Journal Of Core Engineering & Management
Volume-6, Issue-7, 2020 ISSN No: 2348-9510

At 15 degrees angle of attack and U∞ = 48 m/s, the vortex showed addition inboard and upward movement of the vortex core as in figure 13.

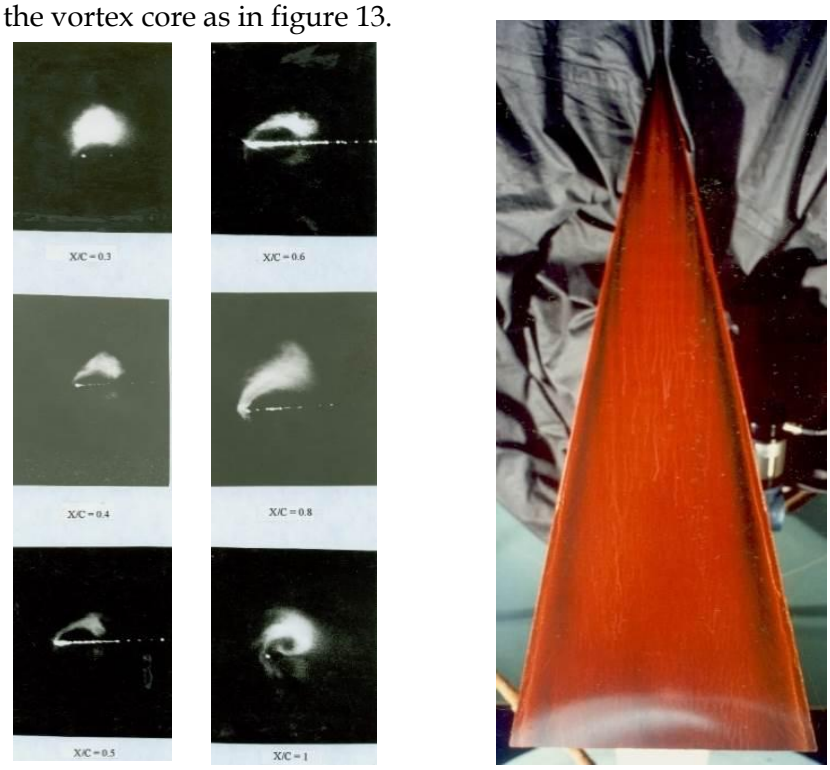

(a) (b)

Figure 9 Flow visualization at zero angle of attack (a, b)

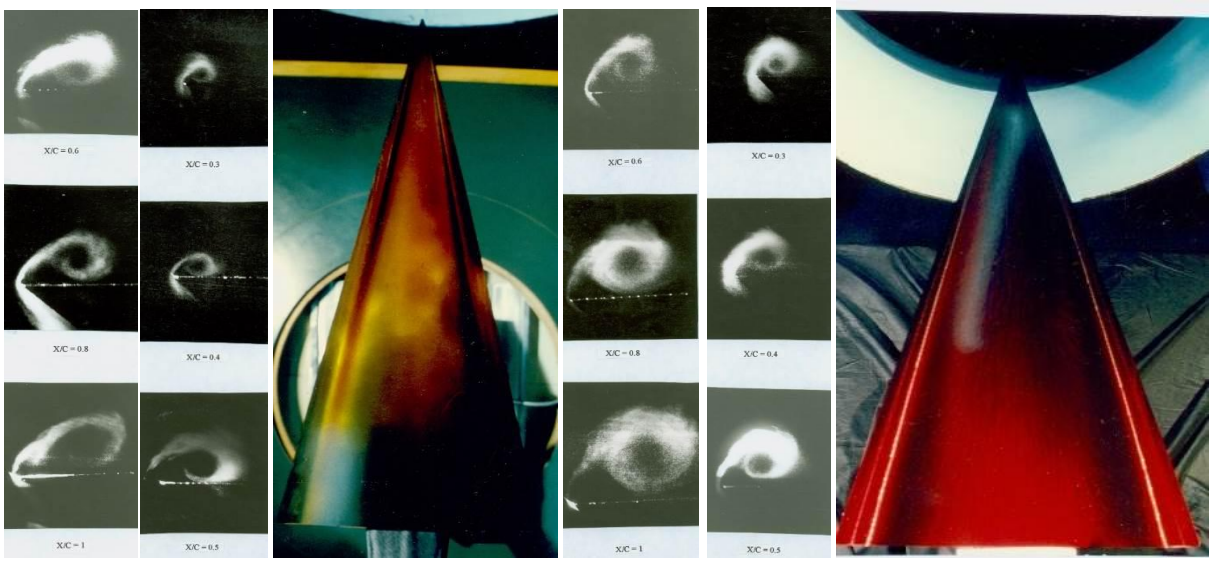

(10- a) (10- b) (11-a) (11-b)

Figure 10, 11 Flow visualization at α=5 degrees (left) and 10 degrees (right) respectively at U∞ = 48 m/s

International Journal Of Core Engineering & Management
Volume-6, Issue-7, 2020 ISSN No: 2348-9510

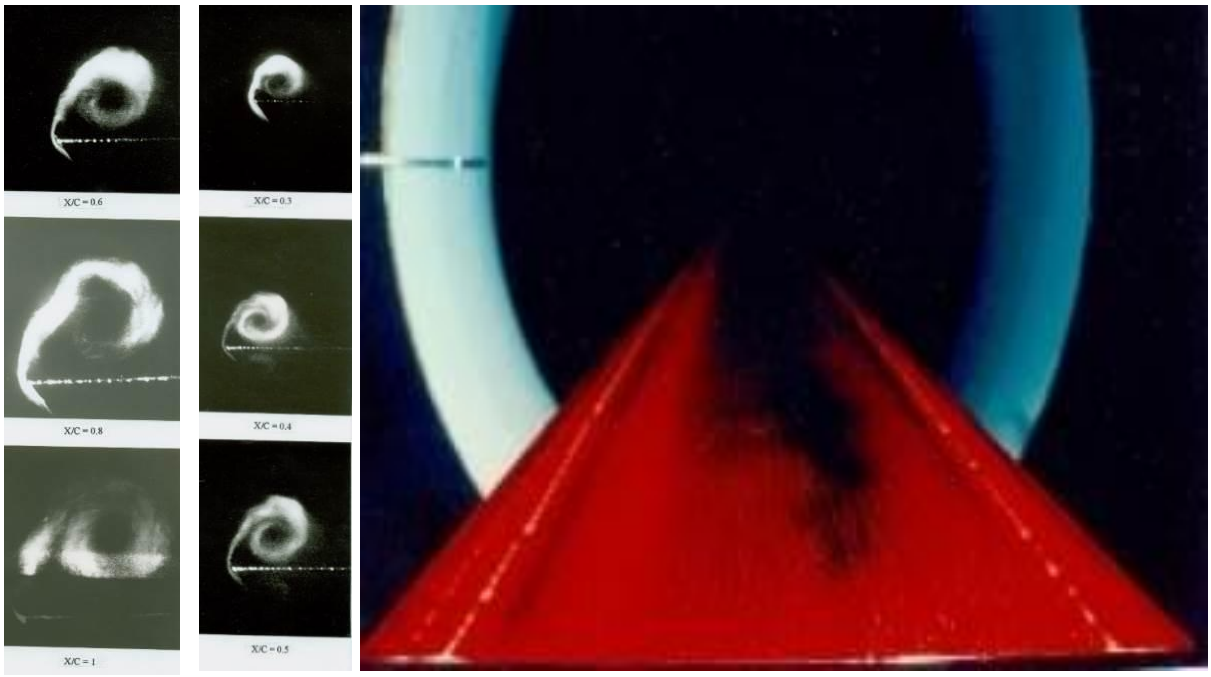

(a) (b)

Figure 12 Flow visualization at 15 degree angle of attack (a, b)

At 20 degree angle of attack and at $U\infty$= 48 m/s, the upstream and upward movement of the vortex is continued (figure 14-a). A laser light sheet crossing the flow parallel to the leeward surface and passing through the vortex subcore on both sides of the wing indicate a good formed vortex subcore and vortex rotational core up to locations beyond the trailing edge (figures 14-b, c). The laminar/turbulent transition of the secondary separation line starts its outward displacement of the secondary separation line from x/Cr=0.426 and y/(S/2)=0.487 up to x/Cr=0.426 and y/(S/2)=0.487 and stay fixed at this location up to the trailing edge (figure 14-d). The obvious deflection of the axial streamlines close to the symmetrical line of the wing toward the symmetrical axial line starts at x/Cr=0.43 (figure 14-d), which is the same location at which the laminar turbulent transition occurs as indication of mutual connection between both phenomena. Dark areas represent regions of high shear stresses as those underneath the vortices (figure 14-d).

International Journal Of Core Engineering & Management
Volume-6, Issue-7, 2020 ISSN No: 2348-9510

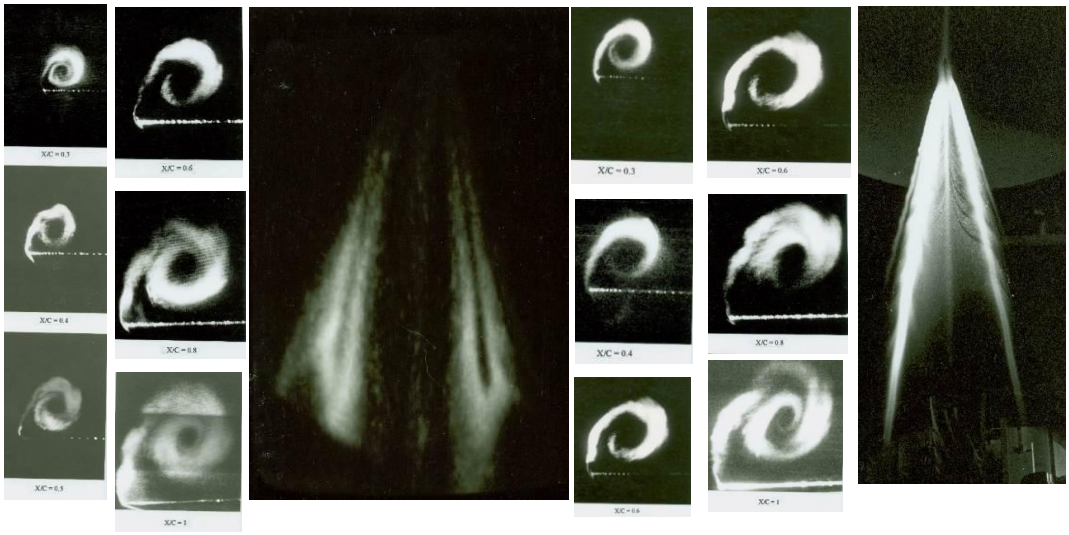

(a) (b) (c) (d)

Figure 13 Flow visualization at 20 degrees angle of attack (a - d)

At 25 degree angle of attack and U∞= 48 m/s, the vortex is healthy and is displaced inboard and upward (figure 15)

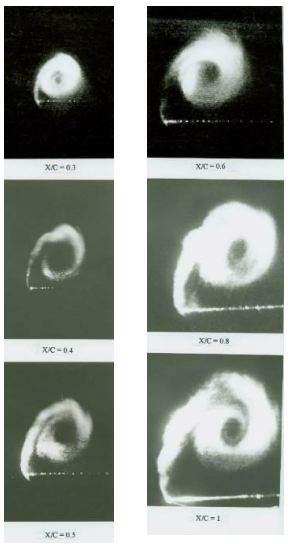

Figure 14 Flow visualization at 25 degree angle of attack.

At 30 degree angle of attack and U∞= 48 m/s, the vortex is continuing its inboard and upward movement with increasing the angle of attack (figure 15-a, e, h). The vortex subcores on both symmetrical sides of the leeward surface are initiated at a common point of x/Cr=0.06 and preserve their healthy condition beyond x/Cr=1.15 (figure 16-b). Both vortex subcores and vortex rotational cores are in a well formed condition up to locations beyond the trailing edge vortexes

International Journal Of Core Engineering & Management
Volume-6, Issue-7, 2020 ISSN No: 2348-9510

(Figure (15-c, d, f, g). The liquid crystal flow visualizations indicate the downstream movement of the laminar/turbulent transition starting at x/Cr=0.353, y/(S/2)=0.248 up to x/Cr=0.412, and y/(S/2)=0.115 on the left side and at 0.37, y/(S/2)= 0.246 up to 0.45, y/(S/2)=0.122 on the right symmetrical side of the wing (figure 15 b-f). The obvious deflection of the axial streamlines, close to the symmetrical line of the wing toward the symmetrical axis, starts at x/Cr=0.36 (figure 15c-f), which is the same location at which the laminar turbulent transition occurs as indication of mutual connection between both phenomena. Two trailing vortices are formed along both trailing edges of both sides of the pressure surface moving upward and when reaching the leeside surface they kink in the direction of the flow over the wing as clearly shown in figures 14-a, c, d, f, g, and figure 17 a, b. The vortex core of the left vortex is straight and healthy even downstream to the trailing edge of the wing while it kinks upward at x/Cr= 0.9 over the wing upward away from the wing as it moves downstream figure 17-a, b. The effect of both trailing vortexes on the surface streamlines are clearly observable in the trailing edge region at y/(S/2)=0.286 to 0.696 on both symmetrical sides of the leeward surface in the form of reversed flow patterns while the dark areas represents regions of high shear stresses as those underneath the vortices (figure 15-a-f, 16-a-d).

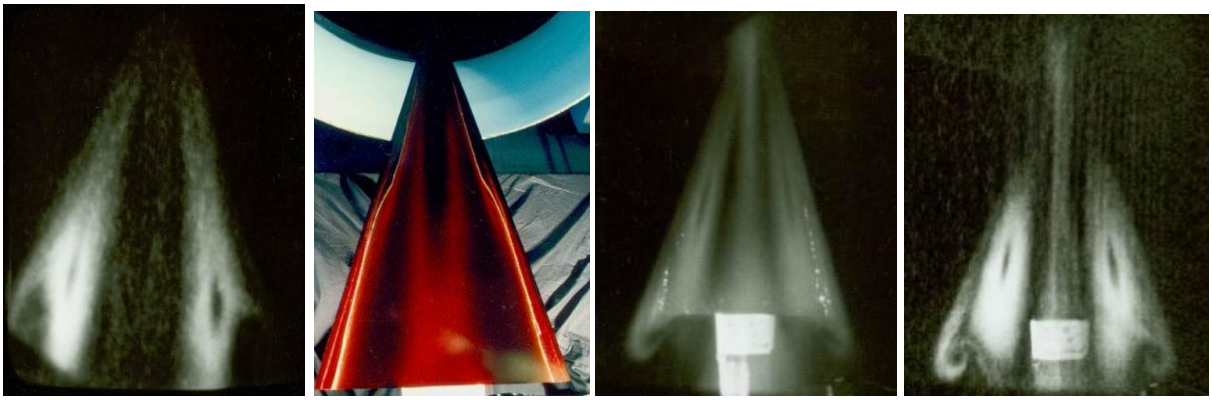

(a) (b) (c) (d)

Figure 16 (a-d) Flow visualization at 30 degree angle of attack

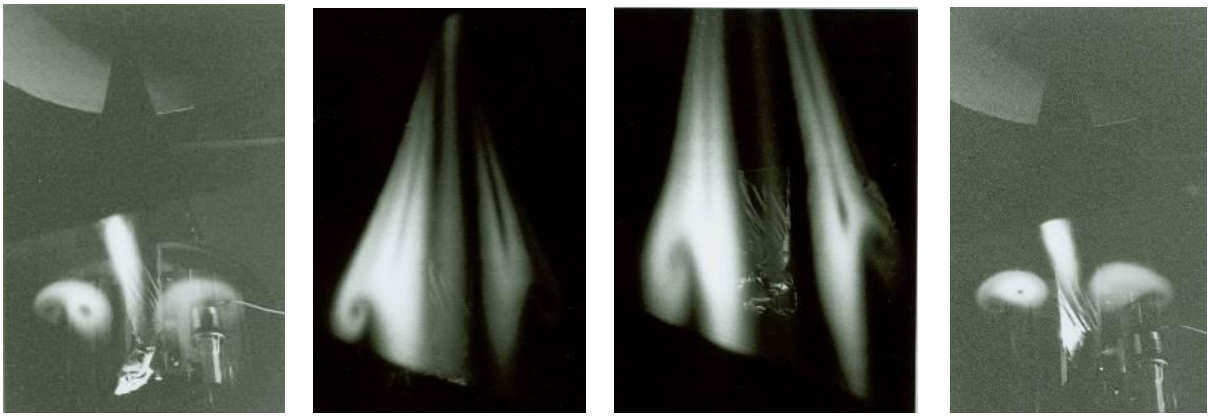

(e) (f) (g) (h)

Figure 15 (e-h) Flow visualization at 30 degree angle of attack

(a)

(b)

Figure 16 Flow visualization at 30 degree angle of attack (a-b)

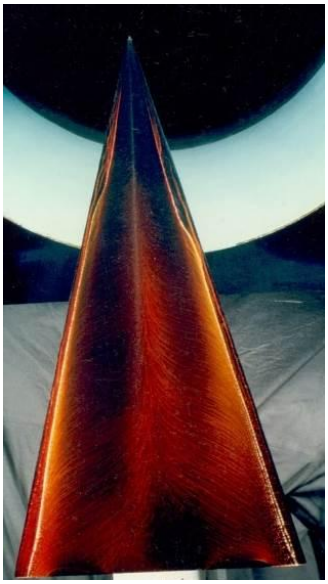

(c)

(d)

Figure 16 Flow visualization at 30 degree angle of attack (c-d)

International Journal Of Core Engineering & Management
Volume-6, Issue-7, 2020 ISSN No: 2348-9510

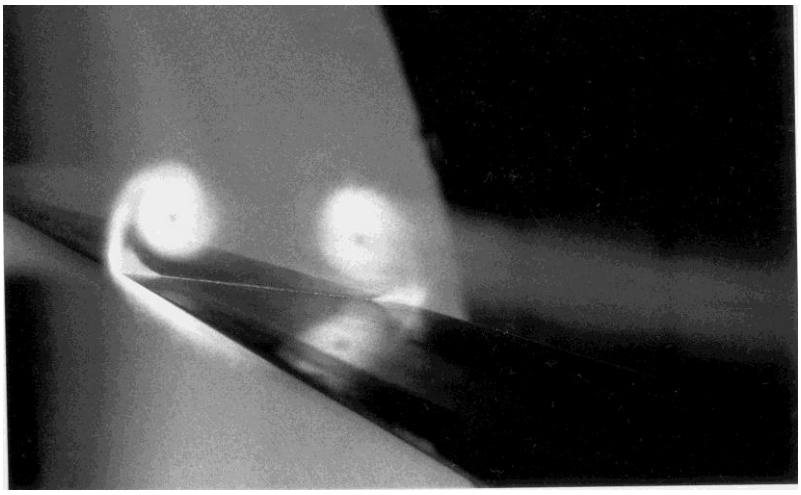

Figure 17-a Smoke/Laser-Light-Sheet Flow visualization at 30 degree angle of attack, X/Cr=0.4

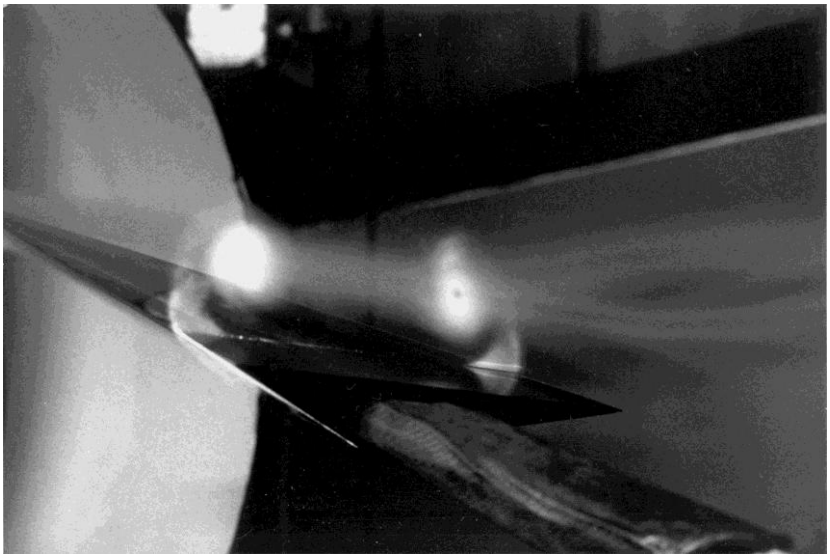

Figure 17-b Smoke/Laser-Light-Sheet Flow visualization at 30 degree angle of attack, X/Cr=0.9

At 32.5 degree angle of attack and U∞= 48 m/s, the smoke/laser-light-sheet flow visualization (figure 18-a) indicates at the lateral cross section of x/Cr=0.4, a primary vortex core at y/(S/2)=0.6 and h/(S/2)=0.45 and a secondary separation at y/(S/2)=0.7 with a secondary vortex core at y/(S/2)=0.87 and h/(S/2)=0.104. The spatial trajectory of the primary vortex subcore indicates a healthy vortex subcore even far downstream of the trailing edge with inward and upward movement by moving downstream of the trailing edge.

International Journal Of Core Engineering & Management
Volume-6, Issue-7, 2020 ISSN No: 2348-9510

The liquid crystal flow visualizations indicate the downstream movement of the laminar/turbulent transition starting at x/Cr=0.321, y/(S/2)= 0.269 up to x/Cr=0.377, and y/(S/2)= 0.114 on the left side and at x/Cr= 0.332, y/(S/2)= 0.267 up to x/Cr=0.407, y/(S/2)= 0.12 on the right symmetrical side of the wing (figure 18-b, c). The obvious deflection of the axial streamlines close to the symmetrical line of the wing toward the symmetrical axial line starts at x/Cr=0.32 (figure 18-c), which is the same location at which the laminar turbulent transition occurs as indication of mutual connection between both phenomena.

Dark areas represent regions of high shear stresses as those underneath the vortices (figure 18 b, c). Two trailing vortices described before are shown in figures 18-c. The effect of both trailing vortexes on the surface streamlines is clearly observable in the trailing edge region at y/(S/2) = 0.355 to 0.839 on both symmetrical sides of the leeward surface in the form of reversed flow patterns (figure 18-b, c, and d).

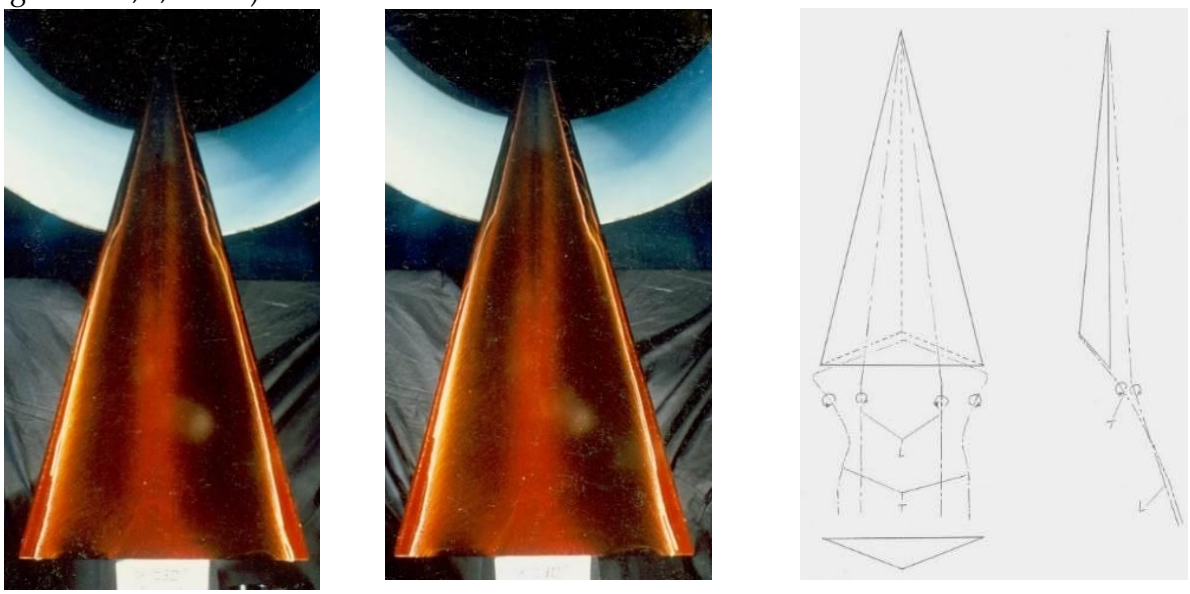

(a) (b) (c)

Figure 18 (c-e) Flow visualization at 32.5 degree angle of attack

At 35 degree angle of attack and U∞ = 48 m/s, the vortex is continuing its inboard and upward movement with increasing the angle of attack (figure 19-a,). Both vortex subcores and vortex rotational cores are observed at x/Cr=0.8 and 0.9 (Figure 19-a). the liquid crystal flow visualizations (figure 19-b) indicate the downstream movement of the laminar/turbulent transition starting at x/Cr=0.29, y/(S/2)= 0.282 up to x/Cr=0.34, and y/(S/2)= 0.11 on the left side and at x/Cr= 0.293, y/(S/2)= 0.277 up to x/Cr=0.36, y/(S/2)= 0.11 on the right symmetrical side of the wing. Dark areas represents regions of high shear stresses as those underneath the vortices. The obvious deflection of the axial streamlines close to the symmetrical line of the wing toward the symmetrical axial line starts at x/Cr=0.29 (figure 19-b), which is the same location at which the laminar turbulent transition occurs as indication of mutual connection between both phenomena. The effect of both trailing vortexes on the surface streamlines are clearly observable in the trailing

International Journal Of Core Engineering & Management
Volume-6, Issue-7, 2020 ISSN No: 2348-9510

edge region at y/(S/2)=0.328 to 0.75 on both symmetrical sides of the leeward surface in the form of reversed flow patterns (figure 19-b).

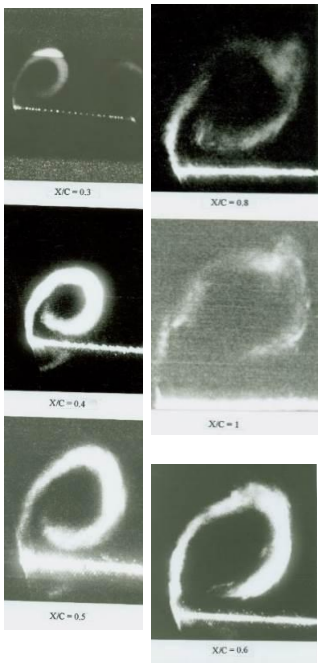

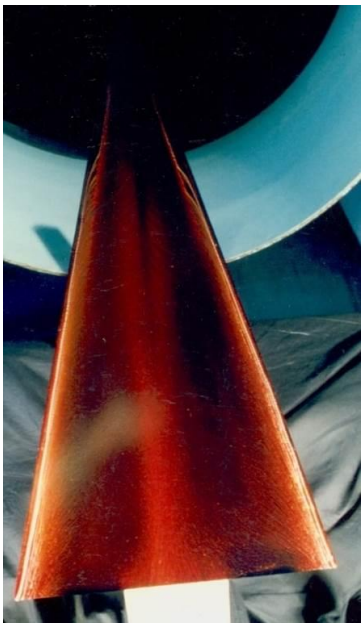

(a) (b)

Figure 18 (a, b) Flow visualization at 35 degree angle of attack

At 40 degree angle of attack, and U∞ = 48 m/s, the vortex is continuing pushing each other inboard and upward competing for the space with increasing the angle of attack (figure 19-a,). Both vortex subcores and vortex rotational cores are weakened at and downstream to x/Cr=0.5 (Figure 19-a). The liquid crystal flow visualizations (figure 19 b) indicate the downstream movement of the laminar / turbulent transition location toward the trailing edge by increasing the angle of attack. The laminar/turbulent transition starts at x/Cr=0.253, y/(S/2)= 0.307 and displaced by moving downstream up to x/Cr=0.307, and y/(S/2)= 0.098 on the left side and at x/Cr= 0.26, y/(S/2)= 0.286 and displaced by moving downstream up to x/Cr=0.32, y/(S/2)= 0.1 on the right symmetrical side of the wing (figure 19-b). Dark areas represent regions of high shear stresses as those underneath the vortices (figure 19-b). The obvious deflection of the axial streamlines close to the symmetrical line of the wing toward the symmetrical axial line starts at x/Cr=0.25 (figure 19-b), which is the same location at which the laminar turbulent transition occurs as indication of mutual connection between both phenomena. The effect of both trailing vortexes on the surface streamlines are clearly observable in the trailing edge region at y/(S/2)=0.333 to 0.75 on both symmetrical sides of the leeward surface in the form of reversed flow patterns (figure 19-b).

International Journal Of Core Engineering & Management
Volume-6, Issue-7, 2020 ISSN No: 2348-9510

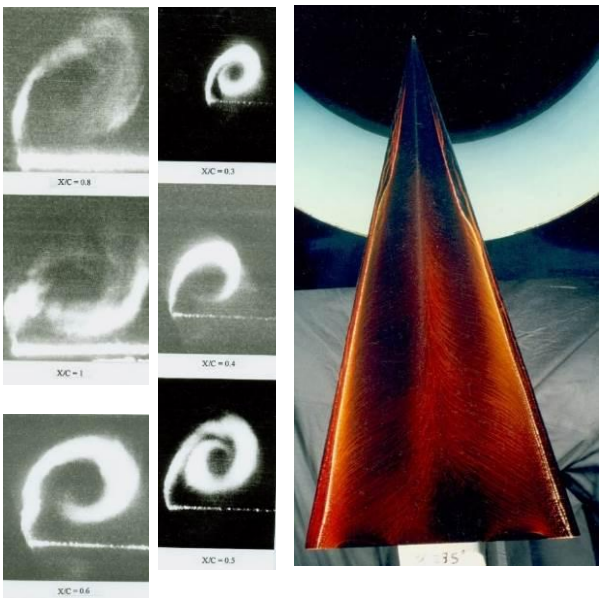

(a) (b)

Figure (19 a, b) Flow Visualization at α=40O

Figure 20 Flow visualization at α=40O.

Increasing the angle of attack to 45 degree at U∞ = 48 m/s results in upstream movement of the vortex breakdown toward the apex (figure 21).

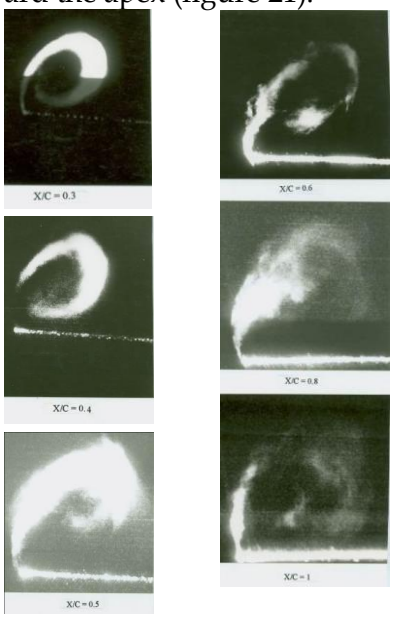

Figure 21 Flow visualization at 45 degree angle of attack.

The Trajectory of the vortex subcore (y/(S/2)) shown in figure 22 based on the laser light sheet flow visualization indicate a continues inboard movement of the vortex subcore from y/(S/2)=0.9 at zero angle of attack toward the axis of symmetry of the leeward surface of the wing by

International Journal Of Core Engineering & Management
Volume-6, Issue-7, 2020 ISSN No: 2348-9510

increasing the angle of attack up to y/(S/2)=0.7 at 10 degrees and remains at this location by further increase in the angle of attack up to 15 degree. The vortex subcore location of the vortex subcore continuous its inboard movement by further increase in the angle of attack up to y/(S/2)=0.65 at 20 degrees angle of attack and remains at this location up to 30 degrees angle of attack. Additional increase in the angle of attack leads to further inboard displacement to y/(S/2)=0.6 at 35 degrees angle of attack and remains at this location up to 45 degrees angle of attack. These results are very consistent and coherent with those obtained from the surface pressures (figure 24).

The Trajectory of the vortex subcore (h/(S/2) shown in figure 24 indicate a linear increase of vertical location of the vortex subcore from the leeward side of the wing with increasing the angle of attack up to 25 degree angle of attack followed by nonlinear increase up to 35 degree and increased slightly by increasing the angle of attack up to 45 degree.

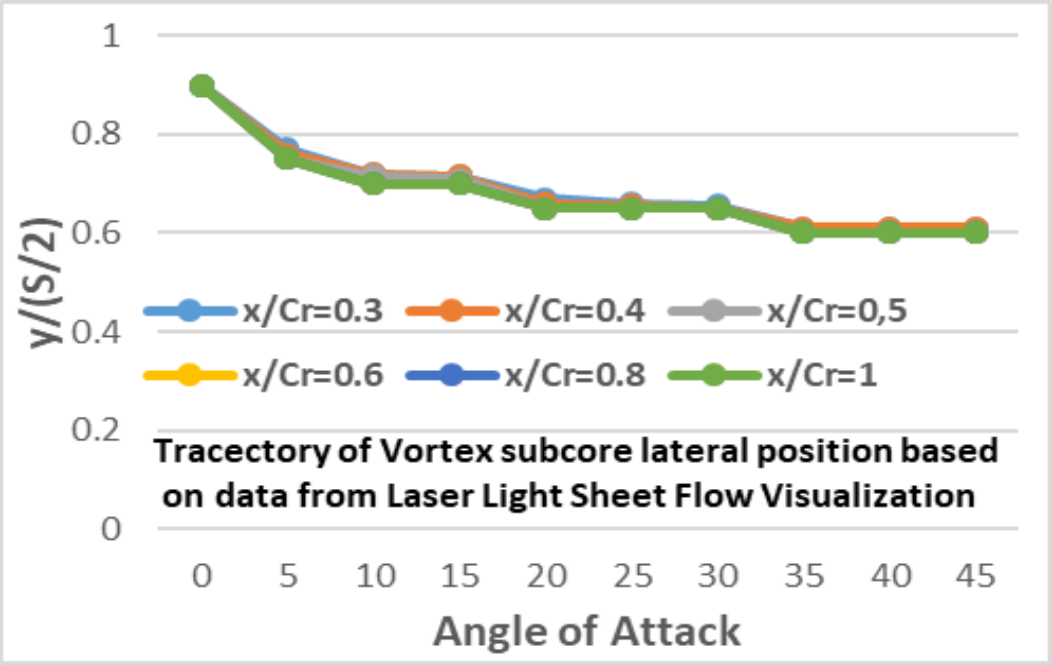

Figure 22 Trajectory of vortex core (y/(S/2)).

International Journal Of Core Engineering & Management
Volume-6, Issue-7, 2020 ISSN No: 2348-9510

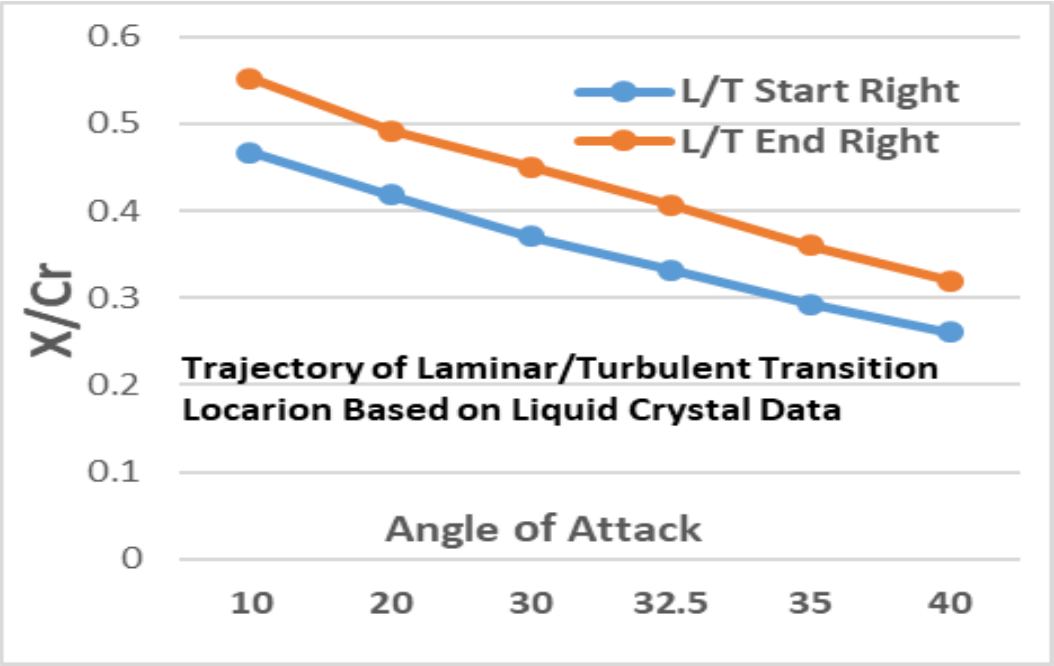

Figure 23 Trajectory of vortex subcore (y/(S/2) based on surface pressures

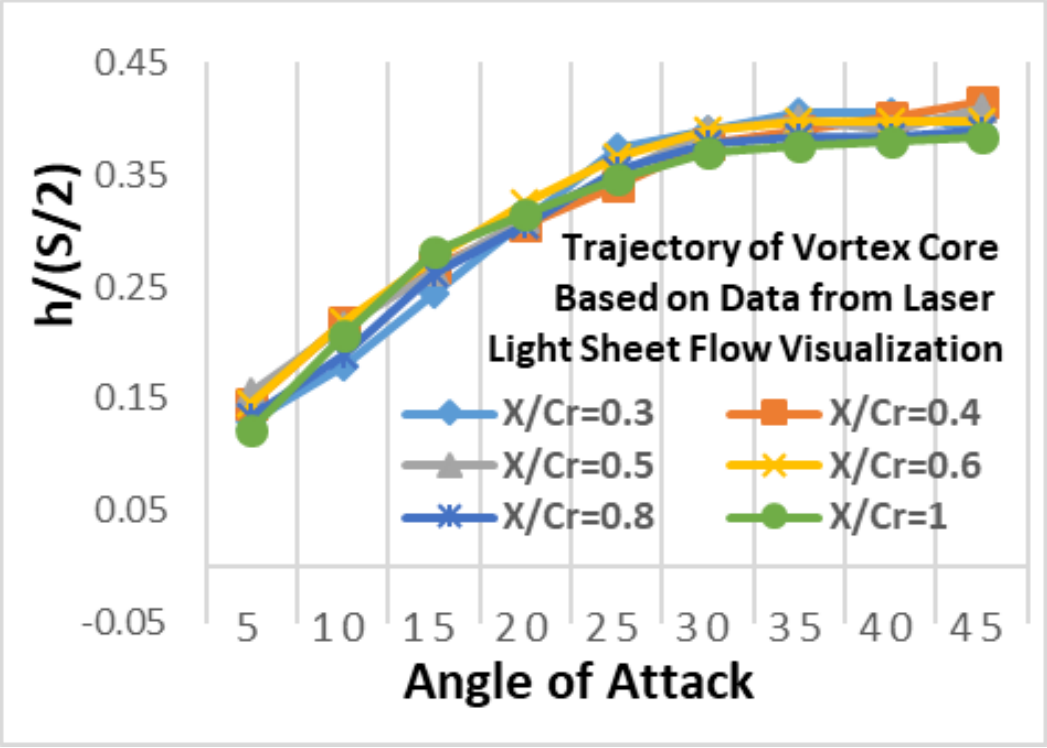

Figure 24 Trajectory of vortex core (h/(S/2))

International Journal Of Core Engineering & Management
Volume-6, Issue-7, 2020 ISSN No: 2348-9510

The downstream location ((x/Cr)), from the wing apex, of the start and end of the outboard kink of the secondary separation line toward the leading edge as indication of the laminar turbulent transition decreases linearly by increasing the angle of attack for the left symmetrical side of the wing (figure 25) as well as for the right symmetrical side of the wing as illustrated in figure 26.

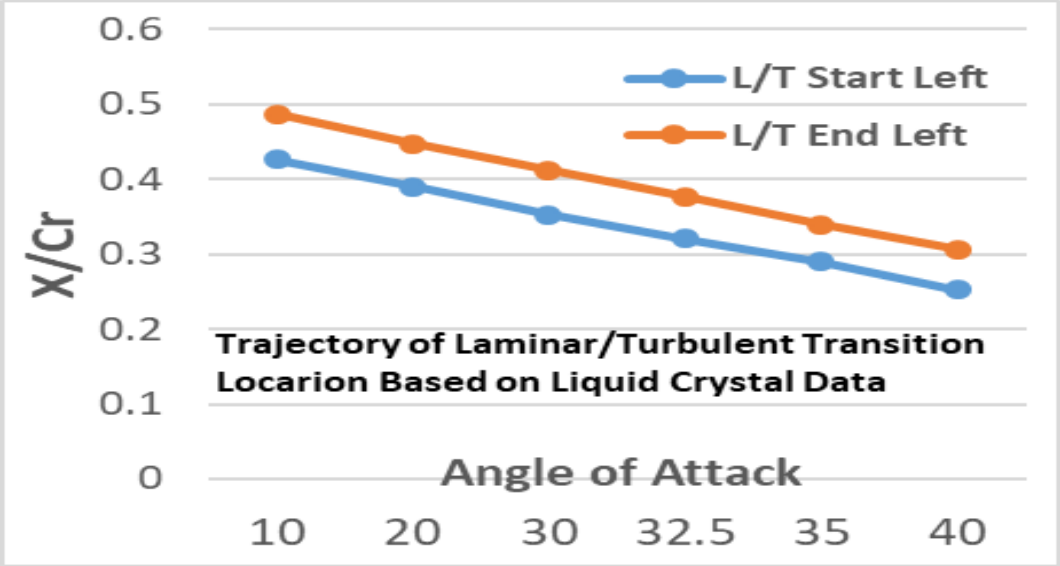

Figure 25 Trajectory of Laminar/turbulent transition (y/(S/2) on the left symmetrical side.

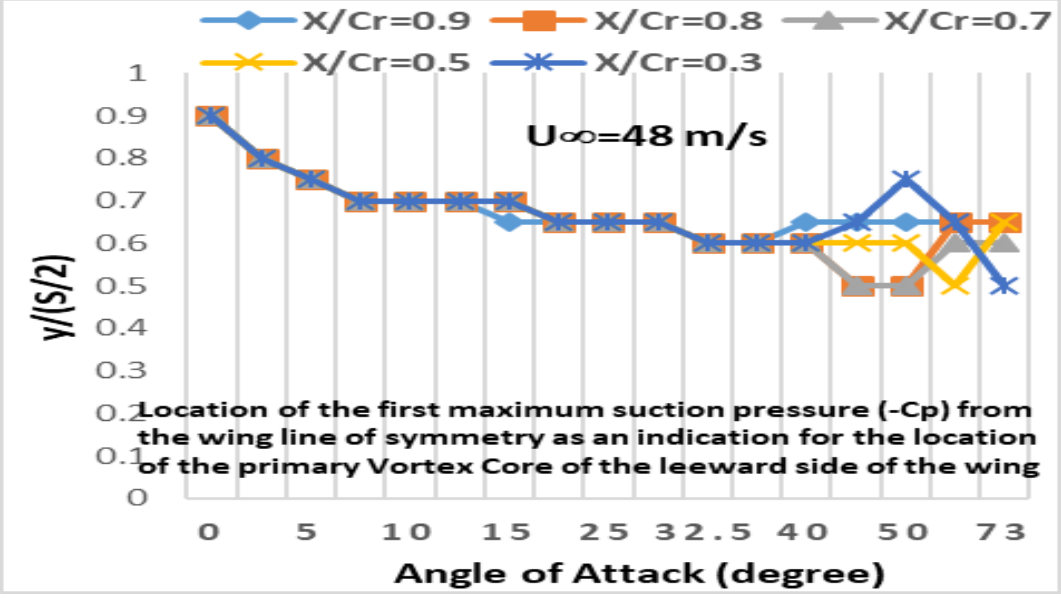

Figure26 Trajectory of Laminar/turbulent transition (y/(S/2) on the right symmetrical side based on experimental surface pressure data

International Journal Of Core Engineering & Management
Volume-6, Issue-7, 2020 ISSN No: 2348-9510

The lateral location (y/(S/2)), from the wing axis of symmetry, of the start of the outboard kink of the secondary separation line toward the leading edge as indication of the laminar turbulent transition region starts and ends at y/(S/2)=0.866 and 0.783 respectively on the right wing side and at-0.874 and -0.786 on the left wing side at 10 degree angle of attack to y/(S/2)=0.9 and 0.714 respectively on the right wing side and at-0.9.2 and -0.7 on the left wing side at 40 degree angle of attack as shown in figure 27.

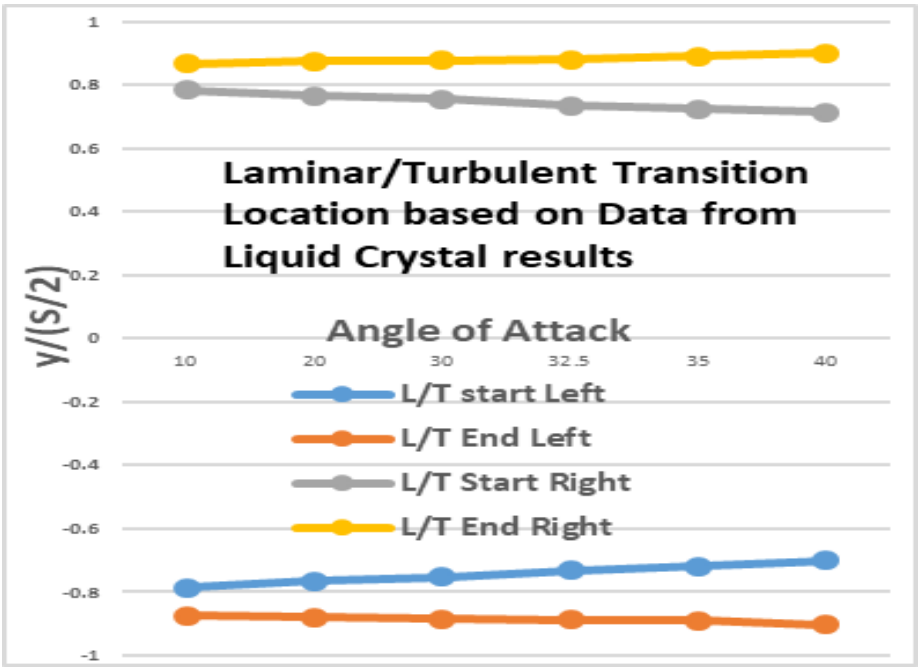

Figure 27 Trajectory of Laminar/turbulent transition (y/(S/2) on the wing

The important software tools which have been used in processing the images were of great assistance in determining the results illustrated in the figures are; numpy (a package for scientific computing with Python [25], matplotlib which is an important library to plot graphs in Python [26], cv2 which is the most used library for computer vision applications in Python [27] and Python programming tool [28] using different techniques described by Hartely R., Zisserman A. (2003) [29]. These results in this investigation will be correlated to the results from other investigation from Omar Salaheldin H. [30]

IV. SUMMARY

In this wind tunnel Investigation, laser light sheet flow visualization is performed at different angles of attack from zero up to 45 degree at free stream speed U∞ = 48 m/s. Also surface streamline visualization is carried out using liquid crystals.

The Trajectory of the vortex subcore (y/(S/2)) based on the laser light sheet flow visualization

indicate a continues inboard movement of the vortex subcore from y/(S/2)=0.9 at zero angle of attack toward the axis of symmetry of the leeward surface of the wing by increasing the angle of attack up to y/(S/2)=0.7 at 10 degrees and remains at this location by further increase in the angle of attack up to 15 degree. The vortex subcore location of the vortex subcore continuous its inboard movement by further increase in the angle of attack up to y/(S/2)=0.65 at 20 degrees angle of attack and remains at this location up to 30 degrees angle of attack. Additional increase in the angle of attack leads to further inboard displacement to y/(S/2)=0.6 at 35 degrees angle of attack and remains at this location up to 45 degrees angle of attack. These results are very consistent and coherent with those obtained from the surface pressure measurements.

A bubble vortex breakdown is observed on the right symmetrical side of the leeward surface with a bubble formed between x/Cr=48 to 0.55 and turbulent flow downstream to this location. On the left symmetrical side of the leeward surface, the disability of the viscous subcore starts at X/Cr=0.35 and increasing downstream up to X/Cr=0.48 forming spirals up to 0.56 followed by turbulent flow structure downstream to this location.

The effect of both trailing vortexes on the surface streamlines are clearly observable in the trailing edge region at y/(S/2)=0.33 to 0.75 on both symmetrical sides of the leeward surface in the form of reversed flow.

The downstream location ((x/Cr)), from the wing apex, of the start and end of the outboard kink of the secondary separation line toward the leading edge as indication of the laminar turbulent transition decreases linearly by increasing the angle of attack for both symmetrical side of the wing.

The lateral location ((y/Cr)), from the axis of symmetry of the leeward surface of the wing, of the start of the outboard kink of the secondary separation line toward the leading edge as indication of the laminar turbulent transition increases linearly with increasing the angle of attack, while the lateral location of the end of this kink decreases linearly by increasing the angle of attack for both symmetrical sides.

REFERENCES

1. Thorpe, S. A. 1968 A method of producing a shear-flow in a stratified fluid. J. Fluid Mech. 32, 693-704.
2. Thorpe, S. A. (1971). Journal of Fluid Mechanics 46: 299{319 (1971).
3. Richardson Lewis Fry (1922). Weather Prediction by Numerical Process, Second Edition, Cambridge University Press, ISBN: 0-521-68044-1 (250pp)
4. Taylor, G. I., (1931). Effect of variation in density on the stability of superposed streams of fluid. Proc. R. Soc. London A, 132, 499–523.
5. Piercy N.A.V. (1923). On the vortex pair quickly formed by some aerofoils, J. R. Aeronaut. Soc. 27 488–500.

6. Winant, C. D.; Browand, F. K. (1974). Vortex Pairing: The Mechanism of Turbulent Mixing-Layer Growth at Moderate Reynolds Number, in: Journal of Fluid Mechanics, pp 237-255, Vol. 63, Part 2, 1974.
7. Earnshaw, P. B (1962). An experimental investigation of the structure of a leading edge vortex. ARC R & M 3281, 1962.
8. Payne, F. M.; Ng, T. T.; Nelson, R. C.; Schiff, L. B. (1986). Visualization and Flow Surveys of the Leading-Edge Vortex Structure on Delta Wing Planforms, AIAA Paper 86-0330, 1986.
9. Payne, F. M. (1987). The Structure of Leading Edge Vortex Flows Including Vortex Breakdown, Ph.D. thesis, Univ. of Notre Dame, Dept. of Aerospace and Mechanical Engineering, Notre Dame, IN, 1987.
10. Nelson, R.C.; Visser K. (1991). Breaking down the delta wing vortex: the role of vorticity in the breakdown process. AGARD, Vortex Flow Aerodynamics 15, 1991.
11. Riley A. J., Lowson M. V. (1998). Development of a three-dimensional free shear layer, J. Fluid Mech. 369, 49.
12. Delery, J. M. (1994) Aspects of Vortex Breakdown, Progress in Aerospace Sciences, Vol. 30, pp. 1-59, 1994
13. Huang X. Z.; Hanff E. S. (1998). Flow Physics of Leading-Edge Vortex-Breakdown, AIAA Paper 98-31536.
14. Earnshaw, P. B.; Lawford, J. A. (1964). Low Speed Wind Tunnel Experiments on a Series of Sharp- edged Delta Wings, R & M 3424, Aeronautical Research Council, August 1964.
15. Michalke, A. (1965). Vortex formation in a free boundary layer according to stability theory, J. Fluid Mech. (1965), vol. 22, part 2, pp. 371-383.
16. Sarpkaya, T. (1971). Vortex Breakdown in Swirling Conical Flows, in: AIAA Journal, pp 1792-1799, Vol. 9, No. 9, April 1971.
17. Leibovich S. (1979). The structure of vortex breakdown, Annual Review Fluid Mech. 10, 221 (1978).
18. Garg, A.K.; Leibovich, S. (1979). Spectral Characteristics of Vortex Breakdown Flow Fields, Physics of Fluids, Vol. 22, No. 11, 1979, pp. 2053-2064. Unsteady Aspects of Leading-edge Vortices RTO-TR-AVT-080 6 -33
19. Hall, M.G. (1972). Vortex breakdown. Ann. Rev. Fluid Mech. 4, 195-218 (1972)
20. Schade, H.; Michalke, A. (1962) Zur Entstehung von Wirbeln in einer freien Grenzschicht, in: Zeitschrift für Flugwissenschaften, Heft 4/5, pp 147-154, Oktober 1962.
21. Faler, J. H.; Leibovich, S. (1977). Disrupted states of vortex flows and vortex breakdown. Phys. Fluids 20, 1385-1400 (1977).
22. Faler, J. H.; Leibovich, S. (1978). An experimental map of the internal structure of a vortex breakdown, J. Fluid Mech. 86, 313 (1978).
23. Lambourne, N. C.; Bryer, D. W. (1961). The Bursting of Leading-Edge Vortices - Some Observations and Discussions of the Phenomenon, Reports and Memoranda 3282,

Aeronautical Research Council, 1961, Reports and Memoranda, Ministry of Aviation: London, United Kingdom, 1961, no. 3282.

24. Ludwieg, H. (1962). Zur Erklärung der Instabilität der über angestellten Deltaflügeln auftretenden freien Wirbelkerne, in: Zeitschrift für Flugwissenschaften, pp 242-249, Heft 6, 1962.
25. Ludwieg, H. (1965). Erklärung des Wirbelaufplatzens mit Hilfe der Stabilitätstheorie für Strömungen mit schraubenlinienförmigen Stromlinien, in: Zeitschrift für Flugwissenschaften, pp 437-442 Heft 12, 1965.
26. Numpy (a package for scientific computing with Python; https://numpy.org/
27. Matplotlib library to plot graphs in Python; https://matplotlib.org/
28. Cv2 library for computer vision applications in Python; https://opencv.org/
29. Python programing tool https://www.python.org/
30. Hartely R., Zisserman A. (2003); Multiple View Geometry in Computer Vision, Second Edition, Cambridge University press.
31. [30] Omar Salaheldin H. (2020); Wind Tunnel Investigation on Surface Pressures and Vortex Flow over Delta Wing at High Angles of Attack and Free-Stream Velocities, International Journal of Core Engineering and Management, Volume 6 , Issue 6, 2020.

Acknowledgement

Great thanks to Mohamad Omar (Futures Educational Systems, https://www.futuresnet.net/) for his important efforts and accomplishments in processing the images using the software tools [25, 26, 27 and 28] in coordination with the authors (1) and (4).